

Reaction blockading in a reaction between an excited atom and a charged molecule at low collision energy

Prateek Puri ¹, Michael Mills ¹, Ionel Simbotin, John A. Montgomery Jr, Robin Côté, Christian Schneider, Arthur G. Suits and Eric R. Hudson, Hudson,

Recent advances have enabled studies of atom-ion chemistry at unprecedentedly low temperatures, allowing precision observation of chemical reactions and novel chemical dynamics. So far, these studies have primarily involved reactions between atoms and atomic ions or non-polar molecular ions, often in their electronic ground state. Here, we extend this work by studying an excited atom-polar-molecular-ion chemical reaction (Ca* + BaCl+) at low temperature in a hybrid atom-ion trapping system. The reaction rate and product branching fractions are measured and compared to model calculations as a function of both atomic quantum state and collision energy. At the lowest collision energy we find that the chemical dynamics differ dramatically from capture theory predictions and are primarily dictated by the radiative lifetime of the atomic quantum state instead of the underlying excited-state interaction potential. This reaction blockading effect, which greatly suppresses the reactivity of short-lived excited states, provides a means for directly probing the reaction range and also naturally suppresses unwanted chemical reactions in hybrid trapping experiments.

ver the past decade, techniques from ultracold physics have been adapted to the study of chemical systems, bringing unique capabilities including precise control of the reagent quantum states and energy1-4. While early work focused on all-neutral chemistry, more recently there has been a shift to the study of charged-neutral reactions⁵⁻⁹, as available techniques allow the probing of a wider range of energy10 and species, as well as trapping and the study of reaction products^{11–13}. These so-called hybrid systems have already been used to study the reactions of several atom-ion combinations^{14–18}, showing a dependence of reactivity on molecular conformation¹⁹ and the production of novel molecules²⁰. Despite this work, there has yet to be a study of atom-polar molecular ion chemistry in these systems. Given that such reactions play a central role in the chemistry of the interstellar medium^{21–23}, which provides the raw materials from which stars, planets and potentially even life developed, understanding these reactions at low temperature is a fundamental goal for chemistry and physics. Moreover, these same reactions could severely limit experiments aiming to produce quantum-state-selected polar molecular ions²⁴⁻²⁶ via sympathetic cool ing^{27-29} for quantum logic applications 30 .

Here, we advance these fronts by using a hybrid trap to study the reaction between electronically excited Ca atoms and BaCl⁺ molecules. Using the capabilities of the hybrid trap, we measure the reaction rates and product branching fractions of these reactions at collision energies from 15 K down to 0.2 K (all temperatures in this work refer to collision energies in units of J/ k_B = K, where k_B is the Boltzmann constant). At the lowest energies in our study, which are among the lowest ever studied in a molecular ion–atom system ^{29,31–33}, we find a chemical regime where the chemical dynamics are primarily dictated by the radiative lifetime of the reagent quantum state instead of the underlying excited-state interaction potential.

Additionally, we provide a simple rule for calculating at what temperature this regime (where the collision time is longer than the radiative lifetime of the quantum state) is reached.

This result parallels previous work in excited-state ultracold neutral-neutral systems where reduced reaction rate constants have been observed and explained as a consequence of spontaneous emission suppressing a short-range excited-state population^{34,35}. Subsequent studies also demonstrated that external optical fields could be used to modify radiative dynamics and directly control the reaction outcome^{36,37}.

The work presented here extends these techniques to the rapidly developing field of cold molecular-ion chemistry. Specifically, the phenomenon observed here should be universal to atom-ion chemical systems and, through its dependence on the reactive trajectory, provides a means to probe the range of a chemical reaction. It also greatly suppresses the reactivity of short-lived excited states. Therefore, this work implies that care must be taken when interpreting low-temperature atom-ion reaction data and that certain unwanted chemical reactions in hybrid trapping experiments can be mitigated by simply moving to low temperatures and thereby allowing longer molecular ion coherence and interrogation times.

In the remainder of this work, we first describe the experimental system and technique for energy control and then present the observed total reaction rates and branching fractions of the Ca $^1\!P_1$ and $^3\!P_2$ states, which show very different behaviours. We then describe a qualitative model for the observed effect that provides a simple means to calculate the temperature at which this radiative regime is reached. Finally, we compare our experimental results to a more rigorous model of the observed effect that is integrated into a modified long-range capture theory.

¹Department of Physics and Astronomy, University of California, Los Angeles, Los Angeles, CA, USA. ²Department of Physics, University of Connecticut, Storrs, CT, USA. ³Department of Chemistry, University of Missouri, Columbia, MO, USA. ⁴UCLA Center for Quantum Science and Engineering, University of California, Los Angeles, Los Angeles, CA, USA. *e-mail: prateek.puri01@gmail.com

ARTICLES NATURE CHEMISTRY

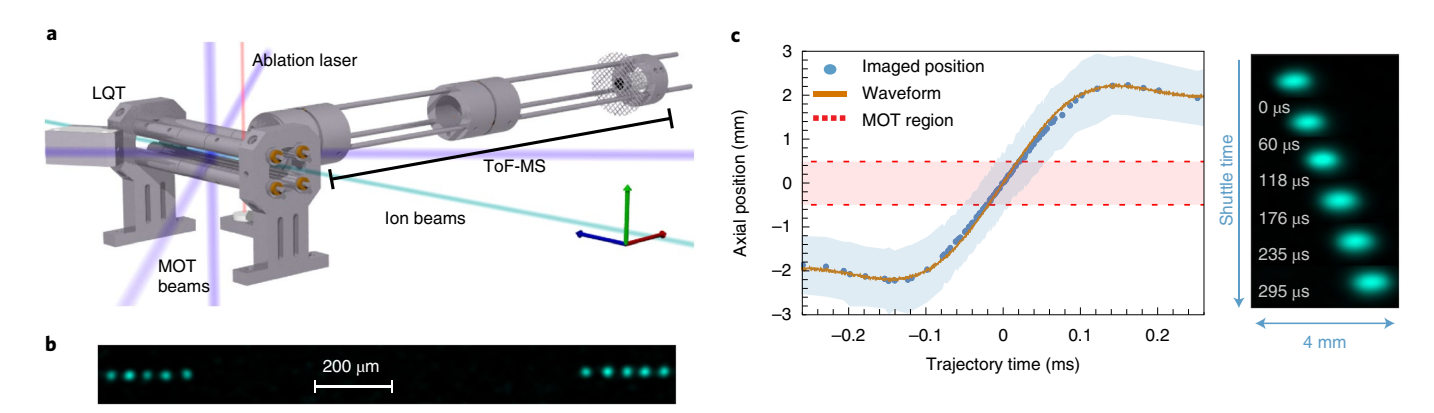


Fig. 1 | Experimental apparatus and techniques. a, The MOTion trap atom-hybrid trap apparatus. **b**, Image of an ion chain being shuttled over a distance of -1 mm at a collision energy of -750 mK. To reduce secular heating, the ions spend over 90% of the time at the trajectory endpoints, and thus ion fluorescence is only visible at these locations. **c**, The trajectory of a shuttled ion sample, as determined by fluorescence images acquired by triggering on the phase of the shuttling waveform. Also presented is the location of the potential minimum of the axial potential as predicted from the endcap waveform voltages at particular instances of time. For reference, the blue shaded region represents the 1/e spatial density width of the 3D Coulomb crystal used in the measurement. The horizontal red shaded region represents the 1/e spatial distance of the MOT cloud. Right, experimental false-colour fluorescence images of the shuttled ions at various times along the shuttling trajectory.

Results

Experimental system. The atom-ion apparatus utilized in this experiment (Fig. 1a), dubbed the MOTion trap and described elsewhere^{20,27,38}, is a hybrid system consisting of a co-located magneto-optical trap (MOT) and a linear quadrupole ion trap (LQT) that is radially coupled into a time-of-flight mass spectrometer (ToF-MS)^{11,12}. Ba⁺ ions are co-loaded into the trap and can be lasercooled to temperatures of ~100 mK to provide sympathetic cooling for the reactant BaCl+ molecules. To tune the reactant collision energy, we employ both a recently developed ion-shuttling technique³⁹ as well as the traditional method of micromotion energy tuning through crystal sample size manipulation^{40,41}. The former technique, which may be used with both three-dimensional (3D) structures and linear ion chains (Fig. 1b), utilizes precise control of the endcap electrode voltages within the ion trap to modulate the position of the ion at a fixed velocity (Fig. 1c). This allows for collision energy scanning without problematic effects associated with micromotion, such as micromotion interruption collisions and poor energy resolution^{42,43}. For the reaction rate data discussed in the following, we implement the technique with 3D structures to increase the data acquisition throughput. Additionally, while not measured directly, we expect that the internal degrees of freedom of the reactant BaCl+ molecules are cooled via sympathetic cooling collisions²⁷ with the Ca MOT.

Observation of reaction blockading. The studied reaction is energetically forbidden in the ground state; however, by using previously established methods involving optical pumping and magnetic trapping, the reaction is shown to proceed via the Ca $^{1}P_{1}$ and Ca $^{3}P_{2}$ electronic states (Supplementary Fig. 1).

After identifying the reaction pathways of the system, the dependence of reaction rate on the collision energy was explored. Atomion chemical reaction cross-sections are typically estimated using a Langevin capture model as $\sigma(E_{\rm col}) = \pi b(E_{\rm col})^2$, where the impact parameter $\sigma(E_{\rm col}) = (\ell+1/2)/(\mu v)$ is determined by the maximum angular momentum $\sigma(E_{\rm col})$ that allows the reaction pair to reach short range at a given collision energy, $\sigma(E_{\rm col})$, where $\sigma(E_{\rm col})$ is the reduced mass of the system and $\sigma(E_{\rm col})$, is subsequently calculated by integrating $\sigma(E_{\rm col})$ over the relative velocity probability distribution of the reaction pair, as $\sigma(E_{\rm col}) = \langle \sigma(E_{\rm col}) v \rangle$. Ultimately, the long-range form of the studied molecular potential determines how the chemical

reaction rate scales with $E_{\rm col}$. For the excited-state systems studied in this work, standard capture theory predicts a reaction rate that increases with decreasing collision energy due to the quadrupole—ion interaction.

To assess this trend in the 3P_2 state, a BaCl+ sample was overlapped with a magnetic trap of pure triplet atoms 20 while micromotion energy tuning was used to change the reactant collision energy from ~ 1 K to 20 K. The measured reaction rate appears to increase at low energy as expected for an ion–quadrupole reaction, as shown in Fig. 2a.

Two methods, excess micromotion energy tuning through crystal size manipulation and ion shuttling, were used to measure the collision energy dependence of the Ca ($^{1}P_{1}$) + BaCl⁺ reaction. Over their common range (4–20 K), the two methods agree and reveal an essentially energy-independent reaction rate constant. However, interestingly, unlike the Ca ($^{3}P_{2}$) state, the measured rate constant decreases at low temperature instead of increasing as predicted by standard quadrupole–ion capture theory (Fig. 2a). All presented theory curves are averaged over the energy distribution of the ions before comparison with the data, and the theory error bands are determined by uncertainties in the polarizability and quadrupole moment values used to construct the molecular potentials utilized in the calculation (see 'Modified capture theory' section for a description of the modified capture theory presented in Fig. 2a).

Branching fraction analysis. Given this departure from standard capture theory, we then measured the product branching fractions to gain a fuller understanding of the chemical dynamics. For experimental convenience, reactions between Ca and non-shuttled BaCl⁺ ions were studied at an average energy of ~5 K. For reactions with the Ca $^1\mathrm{P}_1$ and Ca $^3\mathrm{P}_2$ states, there are three energetically allowed pathways:

$$BaCl^+ + Ca \rightarrow CaCl^+ + Ba$$
 (1)

$$\rightarrow$$
 Ba⁺ + CaCl (2)

$$\rightarrow$$
 Ca⁺ + BaCl (3)

Products from the first two reactions are experimentally identified by the appearance of reaction products in ToF-MS spectra

NATURE CHEMISTRY ARTICLES

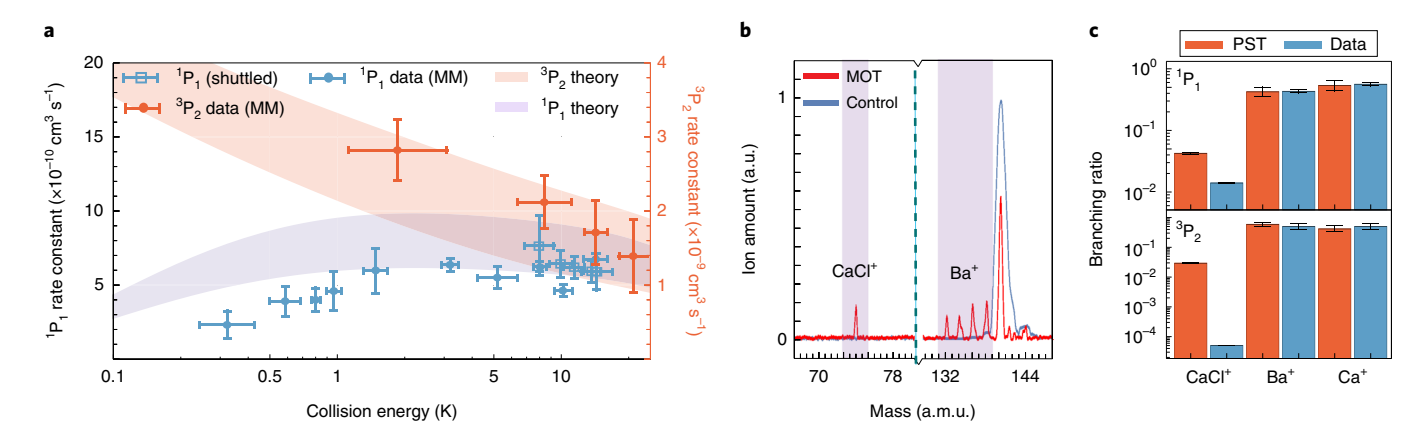


Fig. 2 | Reaction blockading in excited neutral-ion systems. a, Experimental dependence of reaction rate constant on collision energy, as measured through both micromotion (MM) tuning (circles) and shuttling (squares) for both the singlet and triplet reaction surfaces. Note that the *y*-axis scale is different for the two reactions. Both data sets are in reasonable agreement with a modified capture theory incorporating reaction blockading, with the reaction rate of the short-lived Ca ¹P₁ state significantly suppressed at low temperatures as compared to its standard capture theory prediction. For the triplet data, an absolute rate constant is measured at 10 K and all subsequent data points are normalized with respect to this value due to technical difficulties associated with frequent magnetic trap density measurements. Each data point consists of approximately 100 measurements, and error bars are expressed at the one standard error level. **b**, Mass spectra, obtained from ToF-MS, of the identified product ions of the reaction. Shaded areas identify the masses corresponding to the product ions, and a control spectrum is included where the ions were ejected into the ToF-MS without MOT exposure. **c**, A comparison of the measured branching fractions and the predictions of the statistical phase space theory (PST) for both Ca singlet (top) and triplet (bottom) reactions. Experimental error bars are expressed at the one standard error level and, in the case of the CaCl+ values, may be smaller than the marker size.

(Fig. 2b). While the reaction products are created with $\lesssim 1\,\mathrm{eV}$ of energy, the radial (axial) trap depth of the LQT is $\sim 4\,(0.5)\,\mathrm{eV}$ and thus $\geq 95\%$ of charged products are expected to be recaptured in the LQT, assuming isotropic scattering of ions after the reaction. Products from the direct charge exchange reaction (equation (3)) cannot be inferred directly due to a background Ca⁺ influx from MOT atom photoionization; thus, Ca⁺ product branching ratios are inferred indirectly through the presence of the other two products. Additionally, Ba⁺ products are distinguished via their mass from the isotopically pure $^{138}\mathrm{Ba}^+$ coolant ions because the initial BaCl⁺ reactant sample is present in natural abundance.

By monitoring the appearance of Ba⁺ and CaCl⁺ ions in the ToF-MS spectra, branching fractions γ_i , defined as the number of product ions in the ith exit channel formed per BaCl⁺ loss event, are measured. For the 4s4p 1P_1 entrance channel, $[\gamma_{CaCl}^+, \gamma_{Ba}^+, \gamma_{Ca}^+] = [0.014(4), 0.43(6), 0.57(6)], while <math>[\gamma_{CaCl}^+, \gamma_{Ba}^+, \gamma_{Ca}^+] = [0.0001(8), 0.5(2), 0.5(2)]$ is measured for the 4s4p 3P_2 state. Notably, the CaCl⁺ molecule is only definitively detected in 1P_1 reactions, providing a means for quantum state control of the reaction products.

Also shown in Fig. 2c are the branching fractions predicted by a phase space theory calculation⁴⁶. This calculation assumes that all product states that are accessible via energy and angular momentum conservation are equally probable. Thus, product branching fractions are calculated by counting the total number of states available to each reaction product (Supplementary Section 2). The model predicts branching fractions of $[\gamma_{CaCl}^+, \gamma_{Ba}^+, \gamma_{Ca}^+] = [0.04(2), 0.42(17), 0.53(19)]$ for the singlet and $[\gamma_{CaCl^+}, \gamma_{Ba^+}, \gamma_{Ca^+}] = [0.018(14), 0.56(21), 0.41(23)]$ for the triplet, which are in reasonable agreement with the experimental values (Fig. 2c). The error bars are primarily determined by energetic uncertainties in the exothermicity of each reaction channel. The relative ordering of the branching fractions can be attributed to two main factors. First, the CaCl+ exit channel has the lowest product exothermicity and therefore the fewest accessible rovibronic states. Second, the ground state of the CaCl++Ba asymptote is composed of two singlets, whereas the other asymptotes are composed of two doublets, reducing the number of states accessible to CaCl+ by a factor of approximately four.

The relatively good agreement of this model with the data suggests that the reaction proceeds via a long-lived collision complex, which facilitates the realization of ergodicity and therefore the statistical assumption of the model.

Modelling of reaction blockading. Given the evidence for a longlived collision complex from the product branching data and the dramatic difference in reactivity as a function of temperature for quantum states with a long (${}^{3}P_{2}$, $\tau \approx 118$ min) and short (${}^{1}P_{1}$, $\tau \approx 4$ ns) radiative lifetime, the observations suggest that spontaneous emission modifies the chemical dynamics. Because any reaction on an excited surface starts in the separated atom limit, the reagents must propagate inward to short-range separation ($\sim 10 a_0$) before a chemical reaction can occur. If the time it takes to propagate inward to form a collision complex and pass through the transition state to products is similar to the radiative lifetime of the excited reagent, it is likely that spontaneous emission will occur during the chemical event. In this limit, which is more likely at extremely low temperatures, the reactivity of excited reagents will be given by the reactivity of the potential surface reached through spontaneous emission, which in the present case is the endoergic ground-state surface.

To estimate the temperature at which this effect becomes important, it is necessary to calculate the dependence of the total collision time on temperature. Normally, this would be estimated by calculating the lifetime of the three-body collision complex from Rice-Ramsperger-Kassel-Marcus theory^{47,48}; however, this lifetime, which is typically a few vibrational periods, severely underestimates the total collision time at low temperature as it neglects the time it takes for the reagents to fall into the collision complex.

Following similar approaches in neutral–neutral systems³⁶, to account for this effect we consider the collision trajectory of the reactants as they spiral inward along their ground-state and excited-state surfaces. Because these surfaces have different longrange forms due to their differing polarizabilities and quadrupole moments, they diverge from one another as the atom–ion separation distance decreases. This causes any lasers resonant with the system in the dissociation limit to become far-detuned in the region where chemical dynamics occur. At cold temperatures, this effect,

ARTICLES NATURE CHEMISTRY

dubbed reaction blockading, makes it unlikely that the Ca atom will remain in the excited state long enough to react before spontaneously emitting; however, at higher collision velocities, such events are less likely to occur before the atom reaches short range.

This effect is particularly sensitive to the atomic lifetime of the reactive state, as longer excited-state lifetimes allow the reaction complex to reach short range more easily before being interrupted by a spontaneous emission event. As a result, once reaction blockading is integrated into the capture theory predictions, we observe good agreement with the Ca $^1\mathrm{P}_1$ data, whereas for the long-lived triplet state the effect of reaction blockading is negligible, as expected (Fig. 2a).

A more quantitatively rigorous model of the blockading effect is presented in the next section, but we first develop a simple model to estimate when radiative effects become significant. The collision energy $E_{\rm B}$ at which the blockading effect reduces the total reaction rate by half can be approximated by considering the amount of time, $t_{\rm B} = \tau \ln(2)$, it takes to deplete the excited-state population by the same amount, where τ is the excited-state lifetime.

From conservation of energy, $E_{\rm tot} = E_{\rm col}(r) + V_{\rm ex}(r)$, where $E_{\rm tot}$ is the total energy of the system and $V_{\rm ex}(r)$ is the excited-state potential of the system and thus $t_{\rm B}$ can be expressed in terms of the collision energy as

$$\tau \ln(2) = \int_{r_{\rm c}}^{r_{\rm s}} \left(\frac{\mu}{2[E_{\rm tot} - V_{\rm ex}(r)]} \right)^{1/2} dr \tag{4}$$

where $r_{\rm s}$ is the short-range distance at which the chemical event occurs (~50 $a_{\rm 0}$ in our system) and $r_{\rm c}$ is the critical internuclear separation distance where the addressing laser becomes detuned by one linewidth from its associated atomic transition (~1,200 $a_{\rm 0}$ in our system). We obtain $r_{\rm c}$ by solving $V_{\rm ex}(r_{\rm c}) = V_{\rm gs}(r_{\rm c}) + \Delta E - \hbar \Gamma$ where $V_{\rm ex}(r)$ and $V_{\rm gs}(r)$ are the excited-state and ground-state molecular potentials of the system, ΔE is the separation-limit energetic difference between the ground and excited states and Γ is the linewidth of the neutral cooling transition.

Furthermore, if we approximate the velocity, and thus the kinetic energy, of the system as being constant during the latter portion of the trajectory, then $E_{\rm tot} - V_{\rm ex}(r) \approx E_{\rm B}$ and equation (4) can be inverted to yield the final result

$$E_{\rm B} = \frac{1}{\ln(2)^2} \frac{(r_{\rm c} - r_{\rm s})^2}{\tau^2} \frac{\mu}{2}$$

$$\approx \frac{1}{\ln(2)^2} \frac{r_{\rm c}^2}{\tau^2} \frac{\mu}{2}$$
(5)

where $r_s \ll r_c$ in this approximation. Applying equation (5) to the Ca*+BaCl+ system, we calculate E_B to be 560 mK for the 1P_1 state and $\ll 1 \,\mu$ K for the 3P_2 state.

Modified capture theory. For quantitative comparison to the measured rate constant, we require a more rigorous model of the blockading effect than the one presented in the previous section. To this end, we modify standard long-range capture theory to include a probability of reaching short range before spontaneous emission for each partial wave, $P_{\ell}(E_{col}, m_I)$:

$$\sigma(E_{\rm col}) \approx \frac{\pi \hbar^2}{2\mu E_{\rm col}} \sum_{m_{\ell}} \frac{\eta_{m_{\ell}} \chi_{\rm S}}{2J+1} \sum_{\ell=0}^{\ell_{\rm max}(E_{\rm col}, m_{J})} (2\ell+1) P_{\ell}(E_{\rm col}, m_{J})$$
 (6)

where η_{m_j} is the probability that the m_j Zeeman level reacts if it reaches short range, $\chi_{\rm S}$ is the probability that the reaction does not produce an excited BaCl⁺ molecule, and $\ell_{\rm max}(E_{\rm col},m_j)$ is the maximum orbital angular momentum that the entrance system

can possess at energy $E_{\rm col}$ while still being able to reach short range. $P_{\ell}(E_{\rm col},m_f)$ is calculated by simultaneously finding the trajectory of the colliding pair on their interaction potential and solving a two-level Einstein rate equation model to account for electronic population dynamics in the presence of changing electronic energy levels (Supplementary Section 3).

The long-range potentials, assuming the ion to be a positive point charge, are dominated by the ion–dipole polarizability and ion–quadrupole terms, as shown in Fig. 3a,e. As can be seen, for the ${}^{3}P_{2}$ and ${}^{1}P_{1}$ levels the $(J, |m_{j}|) = (2, 2)$ and (1, 0) and $(J, |m_{j}|) = (1, 1)$ states, respectively, have large barriers. Reactants on these potentials cannot reach short range on any partial wave. While the other potentials are attractive at long range, it is necessary to match the long-range potential to the short-range potential energy surface for a complete reaction rate calculation.

To this end, electronic structure calculations were performed using the Gaussian 0949 and Molpro 201250 program packages to calculate the reaction surface for each excited-state reagent, using equation-of-motion coupled cluster theory including single and double excitations (EOM-CCSD) (Supplementary Section 4). The resulting potential surfaces for separation between BaCl+ and Ca ranging from 4 Å and 10 Å are shown in Fig. 3 for the three excited singlet and triplet symmetries, 1A', 2A' and A''. The orange mesh in each panel indicates the asymptotic energy of BaCl⁺ + Ca^{*} - 3.08 eV for the singlet and 1.88 eV for the triplet, neglecting spin-orbit couplings. Most notably, in the case of the singlet, the surfaces corresponding to the 2A' and A'' geometries contain energetic barriers above their respective asymptotic energies at all angles of approach, preventing the reactants from accessing the reaction region at short range. Since only the surface corresponding to the 1A' geometry allows approach to the reaction region, $\eta_{m_1} = 1/3$ for reactions originating in the Ca (1P_1) state. In the case of the triplet, all three surfaces possess a pathway to reach the reaction region. Therefore, given the low temperatures probed here, we take $\eta_{m_i} = 1$ for all reactions originating in the Ca (³P₂) state.

Finally, for the present system there are many inelastic channels that lead to a loss of the initial reagent population, but result in excited states of [BaCl⁺+Ca] that ultimately radiatively decay back into the [BaCl⁺+Ca] ground state, making such reactions indistinguishable from non-reaction events. To estimate the probability of such events, we apply the phase space theory model described earlier (Supplementary Section 2) to the exit channel product [BaCl⁺+Ca]. After including all energetically accessible excited states, we obtain χ_s =0.76(13) and 0.72(17) for the singlet and triplet channels, respectively, with the errors again determined by uncertainties in the exit channel exothermicities (Supplementary Section 2).

The results of this modified long-range capture model, after thermal averaging, are shown in Fig. 2a and are in reasonable agreement with the data. Our model, while capturing the key features of the blockading effect, does not consider non-adiabatic processes that could also play a role in the system. For example, relaxation of the excited-state complex during the collision through internal conversion processes could lead to ground-state reactions and thus a global increase in reaction rate at all studied collision energies. Additionally, the radiative lifetime of the collision complex may change as the system transitions to short range; however, in our model, we assume this lifetime to be constant, fixed by its value in the separated-atom limit.

Discussion

The observed reaction blockading is expected to be a general effect in low-temperature ion-neutral chemistry, as the monopole field of the ion significantly alters the electronic structure of the neutral at relatively long range. Although the modified capture theory developed here can quantitatively treat the suppression effect, the simple expression presented in equation (5) can be used to estimate if reaction

NATURE CHEMISTRY ARTICLES

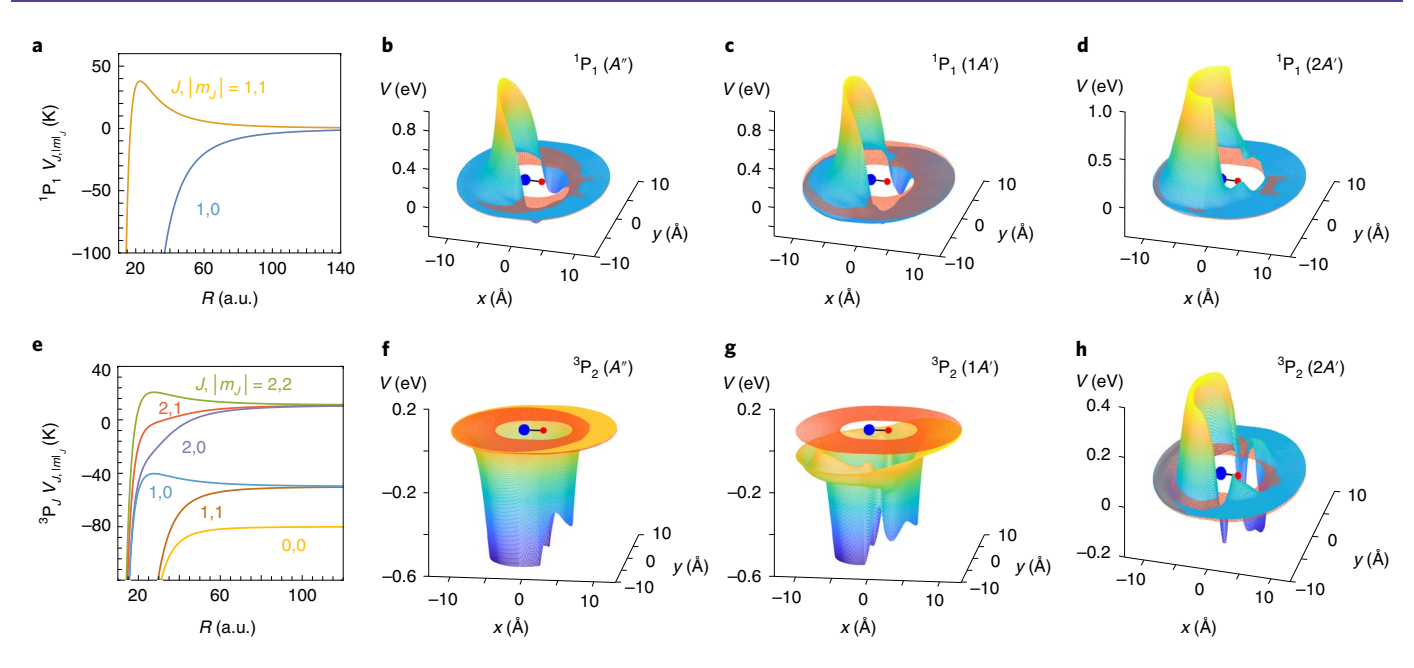


Fig. 3 | Potential energy curves and surfaces. a, Potential energy curves for each $(J, |m_J|)$ level expressed as a function of internuclear separation coordinates for BaCl⁺ + Ca (1 P₁), where the molecular ion is considered as a point charge placed at the origin (Ba⁺ in blue, Cl in orange). **b-d**, Potential energy surfaces corresponding to the A'' symmetry (**b**) and the two A' symmetries (**c**,**d**) for the BaCl⁺ + Ca (1 P₁) complex. The x and y axes are in Å and the z axis in eV. The orange plane is the asymptotic value 3.08 eV above the global ground state of BaCl⁺ + Ca, computed with the same level of theory at R = 50 Å. Short-range energetic barriers along the A'' (**b**) and 2A' (**d**) surfaces prevent the reactants in these surfaces from reaching the reaction region at short range, resulting in a reduction in the overall Ca 1 P₁ reaction rate by a factor of 1/3 (see equation (6)). **e-h**, Similarly for the BaCl⁺ + Ca(3 P₂) complex, potential energy curves (**e**) and surfaces are displayed corresponding to the A'' (**f**) and two A' symmetries (**g**,**h**), with axes consistent with those of the singlet. The orange plane is the asymptotic value 1.88 eV above the global ground state of BaCl⁺ + Ca (singlet) computed with the same level of theory at R = 30 Å. Unlike the Ca 1 P₁ surfaces, no short-range energetic barriers prevent reaching the reaction region for the triplet surfaces and thus there is no additional reduction in triplet reaction rate.

blockading will be important for a given system. For example, in the $(Rb + N_2^+)^{16}$ and $(Rb + Ba^+)^5$ systems studied by the group at the University of Basel, equation (5) predicts that reaction blockading is important at $E \le 10 \, \mathrm{mK}$, significantly below the temperatures of their studies.

In addition to the role reaction blockading may play in the interpretation of low-temperature excited-state reactions, it has an important consequence for the field of quantum-state-selected molecular ions. The reactions studied here represent the dominant loss mechanism for preparing cold molecular ions with laser-cooled neutral atoms²⁸, and the described suppression effect may be critical for enhancing sample overlap times in next-generation hybrid trapping experiments^{30,51}.

In summary, we have presented an investigation of polar molecular ion-neutral chemistry at cold temperature. A recently developed ion-shuttling technique, along with micromotion-energy tuning, was employed to measure the dependence of the reaction rate on collision energy. Branching fractions for the reaction were measured and advanced electronic structure calculations, complemented by a long-range capture theory analysis, were performed to understand the collision dynamics of the system, revealing a strong dependence of the reaction on the approach angle of the incoming Ca atom. We have also demonstrated that spontaneous emission during the collision strongly affects the reaction rate of the system, resulting in a reaction blockading phenomenon. This effect was incorporated into a modified-capture theory model and compared to the experimental data, demonstrating reasonable agreement. A rule of thumb was developed to estimate at what temperature the reaction blockading effect becomes important for a given chemical system. This work builds on previous studies exploring radiative effects in neutral-neutral reactions³⁵⁻³⁷ and represents an important step towards understanding quantum chemical dynamics in hybrid systems as well as controlling such dynamics with optical and electromagnetic fields.

Methods

Experimental apparatus. In a typical experimental sequence, a sample of Ba⁺ and BaCl⁺ ions was loaded into the ion trap by ablating a BaCl₂ target with a pulsed 1,064 nm Nd:YAG laser. The Ba⁺ ions act as a translational sympathetic coolant^{27,51,52} for the BaCl⁺ molecules, enabling the study of reactions at low collision energy. After initialization, the ion crystal was immersed, either while being shuttled or while stationary, in a cloud of roughly two million Ca atoms loaded into an MOT. The ions and atoms were allowed to interact for a variable amount of immersion time before the ions were ejected into the ToF-MS, which registered the amount of each species present in the LQT at a given instant.

Reaction rate measurements. To extract the reaction rate constants, depletion of BaCl+ from the LQT, caused by reactive collisions with the ultracold Ca sample, was monitored as a function of reaction time. In general, the BaCl+ sample may react with several Ca electronic levels that are simultaneously populated, each of which may have differing spatial density distributions and chemical reactivities. Consequently, the reaction kinetics data were fit to a simple rate equation model incorporating the populations and densities of the different electronic states in order to determine a total reaction rate $\Gamma_{\rm T}$ (units of s⁻¹) as

$$\Gamma_{\rm T} = \sum \int \hat{\rho}_{\rm ion}(\mathbf{r}) \eta_i(\mathbf{r}) k_i (E_{\rm col}(\mathbf{r})) \mathrm{d}^3 r \tag{7}$$

where $\eta_i(\mathbf{r})$ is the peak-normalized atom number density of the ith Ca electronic state at position \mathbf{r} , $\hat{\rho}_{\rm ion}(\mathbf{r})$ is the integral-normalized ion-number density evaluated at position \mathbf{r} , and $k_i(E_{\rm col}(\mathbf{r}))$ is the reaction rate constant of the ith electronic state at the spatially dependent collision energy, $E_{\rm col}(\mathbf{r})$. In the case of shuttled ion samples, the ion positions included in the above integral are time-dependent, and thus Γ_T is time-averaged over the experimental duty cycle. Additionally, fluorescence from the laser-cooled Ba+ ions and Ca atoms can be imaged with three separate electron-multiplying charge-coupled device (EMCCD) cameras, allowing for accurate determination of the spatial distributions and densities needed for the rate constant extraction.

ARTICLES NATURE CHEMISTRY

Collision energy control. We used a recently developed ion-shuttling technique to measure how the reaction rate varied with reactant collision energy. Collision energy in hybrid trap experiments is typically controlled by tuning the excess micromotion energy of an ion sample within the LQT; however, while this method allows precise control of the average collision energy, it suffers from poor energy resolution and is susceptible to problematic effects such as micromotion interruption heating. The shuttling method improves on this technique by offering comparatively higher energy resolution while maintaining the ions on the trap null. The essentials of the method are briefly reviewed in the following.

For small displacements around the ion trap centre, the potential in the axial dimension can be approximated as a harmonic oscillator, where offsets in voltages applied to opposing endcap electrodes serve to shift the equilibrium position of the harmonic potential. A time-dependent voltage offset between the endcaps provides precise control of the velocity of the ion, and thus the collision energy, as a function of time. Additionally, the endcap voltage waveforms must be selected carefully to ensure that the ions respond adiabatically to the translating axial potential and experience minimal secular heating.

The position of the ions while shuttling can be tracked for ions with velocities of $\leq 50\,\mathrm{m\,s^{-1}}$ by phase triggering an EMCCD camera on the shuttling waveform and obtaining fluorescence images at various positions along the shuttling trajectory, as shown in Fig. 1b. In this range, the ions follow the waveform predicted trajectory and experience roughly linear motion in the region of intersection with the MOT. Control measurements were taken by monitoring the quantity of ions in the LQT while shuttling for several hundred seconds with no MOT present; these measurements demonstrated that ion loss due to secular heating is negligible.

Data availability

The experimental data sets (displayed in Figs. 1 and 2) are available from the Harvard Dataverse online repository at https://dataverse.harvard.edu/dataverse/cabacl.

Received: 23 October 2018; Accepted: 25 March 2019; Published online: 06 May 2019

References

- Klein, A. et al. Directly probing anisotropy in atom-molecule collisions through quantum scattering resonances. Nat. Phys. 13, 35–38 (2016).
- Carr, L. D., DeMille, D., Krems, R. V. & Ye, J. Cold and ultracold molecules: science, technology and applications. New J. Phys. 11, 055049 (2009).
- Doyle, J. M., Bretislav, F. & Edvardas, N. Physics and chemistry with cold molecules. *ChemPhysChem* 17, 3581–3582 (2016).
- Trippel, S., Stei, M., Cox, J. A. & Wester, R. Differential scattering crosssections for the different product vibrational states in the ion-molecule reaction Ar⁺ + N₂. Phys. Rev. Lett. 110, 163201 (2013).
- Hall, F. H., Aymar, M., Raoult, M., Dulieu, O. & Willitsch, S. Light-assisted cold chemical reactions of barium ions with rubidium atoms. *Mol. Phys.* 111, 1683–1690 (2013).
- Rellergert, W. G. et al. Measurement of a large chemical reaction rate between ultracold closed-shell ⁴⁰Ca atoms and open-shell ¹⁷⁴Yb⁺ ions held in a hybrid atom-ion trap. *Phys. Rev. Lett.* 107, 243201 (2011).
- 7. Zhang, D. & Willitsch, S. Cold Chemistry: Molecular Scattering and Reactivity Near Absolute Zero Ch. 10 (The Royal Society of Chemistry, 2018).
- Ratschbacher, L., Zipkes, C., Sias, C. & Köhl, M. Controlling chemical reactions of a single particle. *Nat. Phys.* 8, 649–652 (2012).
 Silvardy, T. Mair, Z. Pan shlami, R. Alkaman, N. & Oravi, P. Sain.
- Sikorsky, T., Meir, Z., Ben-shlomi, R., Akerman, N. & Ozeri, R. Spincontrolled atom-ion chemistry. *Nat. Commun.* 9, 920 (2018).
- Beyer, M. & Merkt, F. Half-collision approach to cold chemistry: shape resonances, elastic scattering and radiative association in the H⁺+H and D⁺+D collision systems. *Phys. Rev. X* 8, 031085 (2018).
- Schneider, C., Schowalter, S. J., Yu, P. & Hudson, E. R. Electronics of an ion trap with integrated time-of-flight mass spectrometer. *Int. J. Mass Spectrom.* 394, 1–8 (2016).
- Schowalter, S. J., Chen, K., Rellergert, W. G., Sullivan, S. T. & Hudson, E. R. An integrated ion trap and time-of-flight mass spectrometer for chemical and photo-reaction dynamics studies. *Rev. Sci. Instrum.* 83, 043103 (2012).
- Schmid, P. C., Greenberg, J., Miller, M. I., Loeffler, K. & Lewandowski, H. J. An ion trap time-of-flight mass spectrometer with high mass resolution for cold trapped ion experiments. Rev. Sci. Instrum. 88, 123107 (2017).
- Tomza, M. et al. Cold ion-atom systems. Preprint at https://arxiv.org/ abs/1708.07832 (2017).
- Yang, T. et al. Optical control of reactions between water and laser-cooled Be⁺ ions. J. Phys. Chem. Lett. 9, 3555–3560 (2018).
- Hall, F. H. J. & Willitsch, S. Millikelvin reactive collisions between sympathetically cooled molecular ions and laser-cooled atoms in an ion-atom hybrid trap. *Phys. Rev. Lett.* 109, 233202 (2012).
- 17. Zipkes, C., Palzer, S., Sias, C. & Köhl, M. A trapped single ion inside a Bose–Einstein condensate. *Nature* **464**, 388–391 (2010).
- 18. Zipkes, C., Palzer, S., Ratschbacher, L., Sias, C. & Köhl, M. Cold heteronuclear atom-ion collisions. *Phys. Rev. Lett.* **105**, 133201 (2010).

- Chang, Y.-P. et al. Specific chemical reactivities of spatially separated 3-aminophenol conformers with cold Ca⁺ ions. Science 342, 98–101 (2013).
- Puri, P. et al. Synthesis of mixed hypermetallic oxide BaOCa+ from laser-cooled reagents in an atom-ion hybrid trap. *Science* 357, 1370–1375 (2017).
- 21. Stancil, P. C. & Zygelman, B. Radiative charge transfer in collisions of Li with H⁺. *Astrophys. J.* **472**, 102 (1996).
- Smith, D. The ion chemistry of interstellar clouds. Chem. Rev. 92, 1473–1485 (1992).
- Reddy, V. S., Ghanta, S. & Mahapatra, S. First principles quantum dynamical investigation provides evidence for the role of polycyclic aromatic hydrocarbon radical cations in interstellar physics. *Phys. Rev. Lett.* 104, 111102 (2010).
- Calvin, A. T. & Brown, K. R. Spectroscopy of molecular ions in coulomb crystals. J. Phys. Chem. Lett. 9, 5797–5804 (2018).
- Shi, M., Herskind, P. F., Drewsen, M. & Chuang, I. L. Microwave quantum logic spectroscopy and control of molecular ions. *New J. Phys.* 15, 113019 (2013).
- Wolf, F. et al. Non-destructive state detection for quantum logic spectroscopy of molecular ions. *Nature* 530, 457–460 (2016).
- Rellergert, W. G. et al. Evidence for sympathetic vibrational cooling of translationally cold molecules. *Nature* 495, 490–494 (2012).
- Hudson, E. R. Sympathetic cooling of molecular ions with ultracold atoms. EPJ Techn. Instrum. 3, 8 (2016).
- Hauser, D. et al. Rotational state-changing cold collisions of hydroxyl ions with helium. *Nat. Phys.* 11, 467–470 (2015).
- Hudson, E. R. & Campbell, W. C. Dipolar quantum logic for freely-rotating trapped molecular ions. Preprint at https://arxiv.org/abs/1806.09659 (2018).
- 31. Mulin, D. et al. H/D exchange in reactions of OH^- with D_2 and of OD^- with H_2 at low temperatures. *Phys. Chem. Chem. Phys.* 17, 8732–8739 (2015).
- 32. Allmendinger, P. et al. New method to study ion–molecule reactions at low temperatures and application to the reaction. *ChemPhysChem* 17, 3596–3608 (2016).
- Hawley, M. & Smith, M. A. Gas phase collisional quenching of NO⁺ (ν=1) ions below 5 K. J. Chem. Phys. 95, 8662–8664 (1991).
- Julienne, P. S. & Mies, F. H. Collisions of ultracold trapped atoms. J. Opt. Soc. Am. B 6, 2257–2269 (1989).
- Gallagher, A. & Pritchard, D. E. Exoergic collisions of cold Na^{*}-Na. Phys. Rev. Lett. 63, 957-960 (1989).
- Weiner, J., Bagnato, V. S., Zilio, S. & Julienne, P. S. Experiments and theory in cold and ultracold collisions. *Rev. Mod. Phys.* 71, 1–85 (1999).
- Gensemer, S. D. & Gould, P. L. Ultracold collisions observed in real time. Phys. Rev. Lett. 80, 936–939 (1998).
- Schowalter, S. J. et al. Blue-sky bifurcation of ion energies and the limits of neutral-gas sympathetic cooling of trapped ions. *Nat. Commun.* 7, 12448 (2016).
- Puri, P., Mills, M., West, E. P., Schneider, C. & Hudson, E. R. High-resolution collision energy control through ion position modulation in atom–ion hybrid systems. Rev. Sci. Instrum. 89, 083112 (2018).
- Grier, A. T., Cetina, M., Oručević, F. & Vuletić, V. Observation of cold collisions between trapped ions and trapped atoms. *Phys. Rev. Lett.* 102, 223201 (2009).
- Haze, S., Hata, S., Fujinaga, M. & Mukaiyama, T. Observation of elastic collisions between lithium atoms and calcium ions. *Phys. Rev. A* 87, 052715 (2013).
- Chen, K., Sullivan, S. T. & Hudson, E. R. Neutral gas sympathetic cooling of an ion in a Paul trap. *Phys. Rev. Lett.* 112, 143009 (2014).
- 43. Rouse, I. & Willitsch, S. Superstatistical energy distributions of an ion in an ultracold buffer gas. *Phys. Rev. Lett.* **118**, 143401 (2017).
- Dalgarno, A., McDowell, M. & Williams, A. The mobilities of ions in unlike gases. *Phil. Trans. R. Soc.* 250, 411–425 (1958).
- Langevin, P. A fundamental formula of kinetic theory. Ann. Chim. Phys 5, 245–288 (1905).
- Pechukas, P., Light, J. C. & Rankin, C. Statistical theory of chemical kinetics: application to neutral atom–molecule reactions. *J. Chem. Phys.* 44, 794–805 (1966).
- Rice, O. K. & Ramsperger, H. C. Theories of unimolecular gas reactions at low pressures. J. Am. Chem. Soc. 49, 1617–1629 (1927).
- Dagdigian, P. J. Dependence of collision complex lifetime on product internal state: laser fluorescence detection of the Ca+NaCl crossed beam reaction. *Chem. Phys.* 21, 453–466 (1977).
- 49. Frisch, M. J. et al. Gaussian 09, Revision B.01 (Gaussian, 2009).
- Werner, H.-J., Knowles, P. J., Knizia, G., Manby, F. R. & Schütz, M. Molpro: a general-purpose quantum chemistry program package. WIRES Comput. Mol. Sci. 2, 242–253 (2012).
- Staanum, P. F., Højbjerre, K., Skyt, P. S., Hansen, A. K. & Drewsen, M. Rotational laser cooling of vibrationally and translationally cold molecular ions. *Nat. Phys.* 6, 271–274 (2010).
- Rugango, R. et al. Sympathetic cooling of molecular ion motion to the ground state. New J. Phys. 17, 035009 (2015).

NATURE CHEMISTRY ARTICLES

Acknowledgements

This work was supported by grants from the National Science Foundation (PHY-1205311, PHY-1806653 and DGE-1650604) and the Army Research Office (W911NF-15-1-0121, W911NF-14-1-0378 and W911NF-13-1-0213).

Author contributions

P.P. and M.M. acquired and analysed all experimental data presented in the work. P.P evaluated the phase space model for interpreting the experimental branching ratios. I.S., R.C. and P.P. provided the framework for the presented long-range capture model, while J.A.M. performed the electronic structure calculations utilized to understand short-range reaction dynamics. P.P., M.M., I.S., J.A.M. and R.C. contributed to the figures presented in the work. C.S. provided valuable experimental insight, and A.G.S. and E.R.H. provided guidance for the entire project and played key roles in merging the theoretical calculations with the experimental findings. P.P. and E.R.H. prepared the manuscript and all authors provided useful comments.

Competing interests

The authors declare no competing interests.

Additional information

 $\label{eq:supplementary} \textbf{Supplementary information} \ is \ available \ for \ this \ paper \ at \ https://doi.org/10.1038/s41557-019-0264-3.$

Reprints and permissions information is available at www.nature.com/reprints.

Correspondence and requests for materials should be addressed to P.P.

Publisher's note: Springer Nature remains neutral with regard to jurisdictional claims in published maps and institutional affiliations.

© The Author(s), under exclusive licence to Springer Nature Limited 2019